Cite this: DOI: 10.1039/c0xx00000x

www.rsc.org/xxxxxx

ARTICLE TYPE

Layer-by-layer self-assembly of sandwich-like graphene wrapped SnO_x@graphene composite as anode material for lithium ion batteries

Jingjing Tang,[a] Juan Yang,[a] Limin Zhou,[b] Jing Xie,[a] Guanghui Chen,[a] and Xiangyang Zhou*[a]

Received (in XXX, XXX) Xth XXXXXXXXX 20XX, Accepted Xth XXXXXXXXX 20XX

DOI: 10.1039/b000000x

Sandwich-like hybrid nanosheets consisting of graphene wrapped SnO/SnO_2 nanocrystals anchored on graphene have been synthesized via a facile layer-by-layer self-assembly approach. The hierarchical structure exhibits good cyclability and rate performance benefiting from the unique double protection of graphene layers.

Lithium ion batteries have been widely used in portable electronic devices since the commercialization of the first generation by Sony in 1991, and they are considered as one of the most promising energy storage devices for electric vehicles and hybrid electric vehicles.[1-3] Because of the urgent demand for rapid development of such applications, lithium ion batteries with high energy density and long cycle life are intensively required. It is well known that the performance of lithium ion batteries largely depends on the physical and chemical properties of the electrode materials.[4] High energy density batteries can be achieved by utilizing electrode materials with high specific capacities.[5] At present, the lamellar structure of graphitic carbon materials are often employed as anode materials in lithium ion batteries, which can avoid the problem of lithium dendrite formation, guarantee good cyclability and safety. However, the current commercial graphite with a limited theoretical lithium storage capacity (372 mAh g^{-1}) can hardly meet the demand for high energy density batteries.[6] In recent years, extensive research focuses on developing alternative anode materials to realize a high specific capacity and good cyclability, such as metals, metal oxides, metal sulphides and non-metal materials reported before.[7-14] Among them, SnO_x (x=1, 2) has attracted significant attention due to the high theoretical lithium storage capacity (782 mAh g^{-1} for SnO_2, 875 mAh g^{-1} for SnO).[10,15,16] Notwithstanding, the commercial application of SnO_x anodes is hindered due to the poor electrical conductivity and dramatic capacity fading caused by the large volume expansion/contraction during the alloying/dealloying reaction of SnO_x with lithium.[17] Therefore, it is significant to have morphology and structure modification to improve the electrochemical performance of SnO_x.

The incorporation of carbon matrix is regarded as a feasible way to improve the cyclability and rate performance of SnO_x-based anode materials ascribed to the intrinsic good electrical conductivity and stress-buffering nature of carbon.[18-20] Since the discovery of graphene in 2004, it has sparked exciting research interest in the science and technology of two-dimensional nanomaterial. Due to the excellent electrical conductivity, high carries mobility, high mechanical strength and large surface area, graphene is regarded as a superior carbon matrix.[21,22] Recently, many attempts have been made to decorate SnO_x on graphene to obtain enhanced electrochemical performance and the comparison of the electrochemical performance of SnO_x/graphene is shown in Table S1 (ESI†).[23-25] However, to the best of our knowledge, there is almost no report on synthesis of sandwich-like graphene/SnO_x/graphene hybrid nanomaterial via a facile approach.

Herein, we provide a layer-by-layer self-assembling approach to synthesis sandwich-like graphene wrapped SnO_x@graphene (SnO_x@G/G) composite. SnO_2 and SnO are selected as the research objects due to their low intercalation potential for lithium ions and the high theoretical specific capacity. Sandwich structure is expected to assure solid contact between SnO_x and graphene layers, provide a continuous conductive path between SnO_x particles, and accommodate the volume changes during the lithiation and de-lithiation process. The representative fabrication procedure is illustrated in Scheme 1. Graphene oxide (GO) was synthesized from graphite powder based on modified Hummer's method.[26] Due to the electrostatic adsorption of Sn^{2+}, SnO_2 was readily generated on negative charged GO to form SnO_2@GO. Then SnO_2@GO was positively charged by the modification of polydiallydimethylammonium chloride (PDDA) with electron-withdrawing ability to prepare p-SnO_x@GO.[27] Due to the electrostatic interaction between p-SnO_x@GO and GO, a sandwich-like GO enwrapped SnO_x@GO was fabricated. Hydrazine was employed as a reducing agent to get the final SnO_x@G/G composite. For comparison, SnO_2@G was prepared through the chemical reduction of SnO_2@GO by hydrazine. Detailed experimental section is available in ESI†.

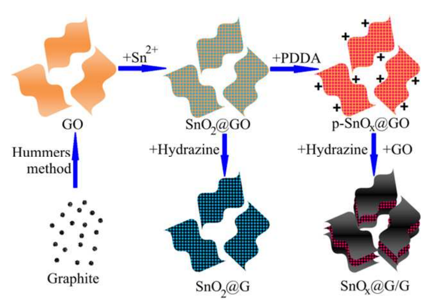

Scheme 1 Schematic illustration of the stepwise synthesis of SnO_2@G and SnO_x@G/G.

The crystalline phases of the as-prepared SnO_2@G and SnO_x@G/G were identified by X-ray diffraction (XRD) as displayed in Fig. 1a. For the XRD pattern of SnO_2@G, the well resolved diffraction peaks located at 26.5°, 33.7°, 37.9°, 51.6°, 61.6° and 65.5° are assigned to the (110), (101), (200), (211), (310) and (301) planes of SnO_2 structure. However, the XRD characterizations confirm the formation of SnO in the SnO_x@G/G due to the appearance of diffraction peaks located at 29.8°, 33.3°, 37.1°, 47.8°, 50.7° and 57.3°, ascribed to the (101), (110), (002), (200), (112) and (211) planes of SnO, respectively. The XRD patterns of SnO_2@GO and p-SnO_x@GO displayed in Fig. S1 (ESI†) demonstrated that SnO_2 can be transformed to SnO nanocrystals during the modification of PDDA. To the best of our knowledge, this transformation has never been reported before and the exact mechanism needs to be further studied. The Fourier transform infrared (FT-IR) spectra of samples as shown in Fig. 1b reveal how the molecular structure changed during the assembly process. The strong peak at 603 cm^{-1} was assigned to Sn-O bond. For p-SnO_x@GO, the peaks located between 1500 cm^{-1} and 1300 cm^{-1} are ascribed to the functionalization of PDDA.[27,28]

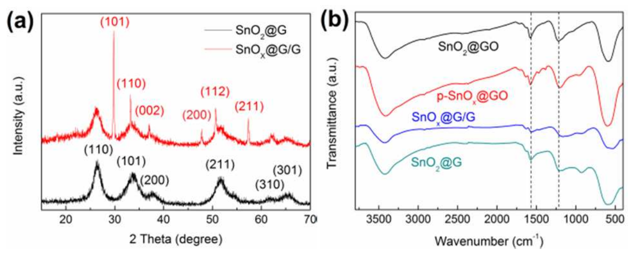

Fig. 1 (a) XRD pattern of SnO_2@G and SnO_x@G/G. (b) FT-IR spectra of SnO_2@GO, p-SnO_x@GO, SnO_x@G/G and SnO_2@G.

Raman spectroscopy is another powerful method to analyze crystal structure and crystal phase. Fig. S2 (ESI†) displays the Raman spectra of SnO_2@G and SnO_x@G/G. The strong peaks located at around 1360 and 1590 cm^{-1} correspond to the typical D-band and G-band of carbonaceous materials. The Raman shifts at 493, 626, 751 cm^{-1} can assigned to the fundamental Raman active modes of SnO_2. Besides, the peak position at 208 cm^{-1} assigned to the SnO active mode,[29] further demonstrating the existence of SnO for SnO_x@G/G. Since the fact that SnO is solvable in HCl solution and SnO_2 is stable upon calcinations in air, the content of SnO, SnO_2 and graphene in the composite is determined based on acid treatment and thermogravimetric analysis (TGA).[10] The content of SnO in SnO_x@G/G is approximately 20 wt% by the dissolution of diluted HCl solution. The contents of SnO_2 in SnO_x@G/G and SnO_2@G calculated based on TGA curves (Fig. S3, ESI†) are 58 % and 80 %, respectively.

The morphology and structure of the SnO_x@G/G were elucidated by scanning electron microscopy (SEM) and transmission electron microscopy (TEM) observations as shown in Fig. 2. SEM images (Fig. 2a and b) of SnO_x@G/G show that the obtained hybrid material presents a free-standing sheet-like structure with a lateral size up to 1 μm. Fig. 2c and d displays the low magnification TEM and high resolution TEM (HRTEM) images of SnO_x@G/G. The fuzzy edges of SnO_x@G/G as shown in Fig. 2c proved that the SnO_x@G is perfectly enwrapped by graphene through the electrostatic interaction of negatively charged GO and positively charged p-SnO_x@GO. By contrast, TEM image of SnO_2@G (Fig. S4, ESI†) confirms that the SnO_2 nanocrystals are fully grafting onto the graphene surface without the additional graphene edges. The crystal structures of SnO_2 and SnO nanoparticles are revealed by the HRTEM acquired from the edges of SnO_x@G/G as shown in Fig. 2d, which is in accordance with the XRD patterns. The lattice spacings of 0.334 nm and 0.298 nm are ascribed to the (110) plane of SnO_2 crystals and (101) plane of SnO crystals, respectively.

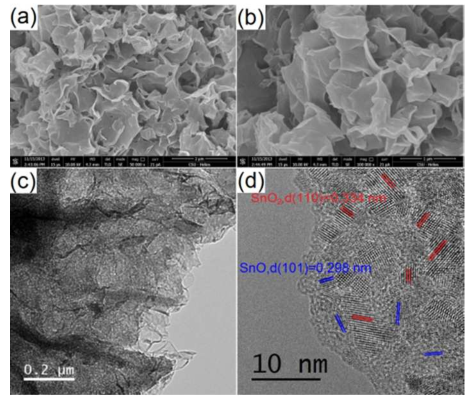

Fig. 2 (a and b) SEM and (c and d) TEM images of SnO_x@G/G.

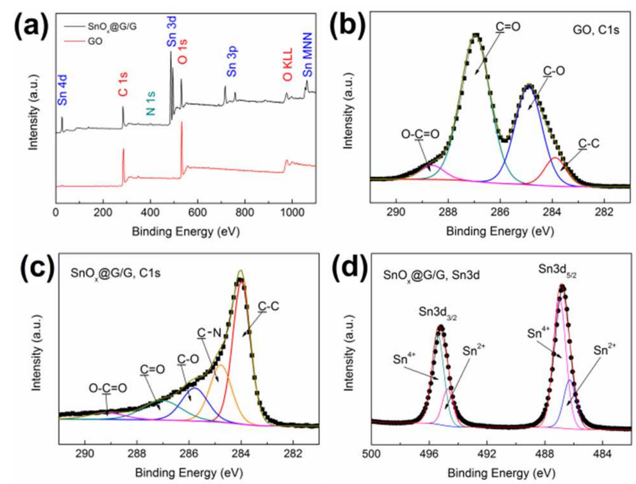

Fig. 3 (a) Survey XPS spectra of GO and SnO_x@G/G. C1s XPS spectra of (b) GO and (c) SnO_x@G/G. Sn3d XPS spectra of (d) SnO_x@G/G.

X-ray photoelectron spectroscopy (XPS) was employed to get insight into the chemical bonding environment (Fig. 3). For GO, the percentage of oxygen based on XPS survey spectrum is around 39.5 % and the deconvolutions of the C1s are fitted by four component peaks, which are assigned to C-C, C-O, C=O and O-C=O functional groups.[30] In the case of SnO_x@G/G, four elements (C, O, N, Sn) were distinguished in the survey XPS spectrum. N species were introduced because of the modification of PDDA (R-N^+ groups of PDDA) and the reduction of hydrazine, which is beneficial to enhance the electrochemical performance of N-doped graphene-based materials.[31,32] The intensity of C-O, C=O and O-C=O band become much weaker in comparison with that of GO as shown in Fig. 3c, indicating the removal of most oxygen functionalities. In addition, the deconvolutions of the Sn3d demonstrate the existing of Sn^{2+} and Sn^{4+} species in

SnO_x@G/G,[33] which is in good agreement with the previous analysis.

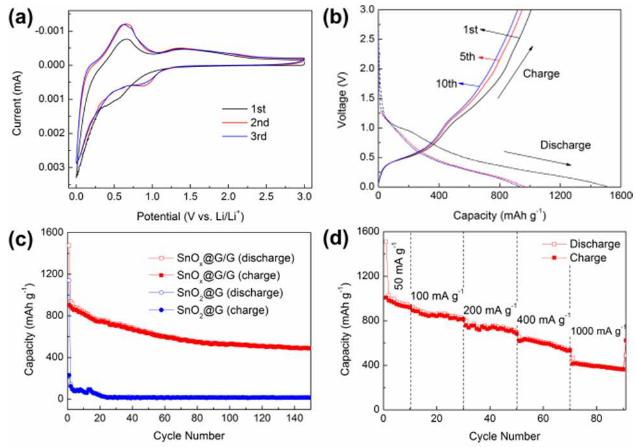

Fig. 4 (a) Cyclic voltammetry curves of the SnO_x@G/G. (b) Voltage profiles of the SnO_x@G/G composite of 1st, 5th and 10th cycles. (c) The cycling performances of the SnO_x@G/G and SnO_2@G at 200 mA g^{-1}. (d) Rate performance of SnO_x@G/G.

The electrochemical performance of SnO_x@G/G was evaluated by the assembly of lithium half-cells. Cyclic voltammetry (CV) was carried out at a scan rate of 0.5 mV s^{-1} in the voltage range of 0.005-3 V. As shown in Fig. 4a, the appearance of the CV profiles of the SnO_x@G/G composite resembles to other reported SnO_2-based composites.[34,35] In the initial cathodic sweep, two reduction peaks can be observed at 0.58 V and 0.005 V. The former peak is formed by irreversible lithium insertion process, such as the transformation of SnO_x to Sn and the formation of a solid electrolyte interface (SEI). This peak is not present in the following cycles. The latter peak could be attributed to the formation of Li_xSn alloys and Li_xC_6 composites. In the first anodic sweep process, three peaks observed at 0.15, 0.66 and 1.37 V are ascribed to the reversible lithium extraction from the SnO_x@G/G composite. The peak position and the intensity are fairly stable for the subsequent cycles indicating the good electrochemical stability of SnO_x@G/G. Fig. 4b shows the discharge/charge profiles at typical cycles of SnO_x@G/G at a current density of 50 mA g^{-1}. The initial discharge and charge capacity of the hybrid are 1509 and 1007 mAh g^{-1}, respectively, giving a coulombic efficiency of 66.7 %. The irreversible capacity in the first cycle is mainly attributed to the formation of Li_2O and SEI layer, which is in agreement with the CV studies. In the subsequent cycles, the discharge plateau at 0.58 V cannot be detected, indicating that the irreversible change mainly occurs in the initial cycles. The columbic efficiency of the hybrid increased to 98.5 % after 10 cycles, delivering a charge capacity of 919 mAh g^{-1}. The cycling performances of SnO_x@G/G and SnO_2@G cycled at a current density of 200 mA g^{-1} are compared as shown in Fig. 4c. The SnO_x@G/G composite delivers a capacity of 1474 mAh g^{-1} in the first discharge and 904 mAh g^{-1} in the first charge process, while SnO_2@G gives a capacity of 1140 mAh g^{-1} in the first discharge and 230 mAh g^{-1} in the first charge process. Besides, the capacity of SnO_2@G decreases continuously due to the large volume change during the cycling. However, the SnO_x@G/G composite exhibits much higher reversible capacity than that of SnO_2@G. The reversible capacity of SnO_x@G/G maintains at 530 mAh g^{-1} after 100 cycles. The coulombic efficiency of the first cycle is 61.3%, but is above 95% after the second cycle and above 98.8 % after 80 cycles, indicating the good capacity retention. It is well known that the metal oxide-based materials suffer from huge volume changes during the lithiation and de-lithiation process. The consequent mechanical strain can cause the collapse of the electrode materials and the loss of contact between active materials and current collector, which is responsible for the fast capacity fading upon cycling. The better electrochemical performance of SnO_x@G/G than that of SnO_2@G is attributed to the unique sandwich structure, which effectively provided an elastic buffer space to accommodate the volume changes during cycling and secured the SnO_x nanocrystals between graphene layers. Meanwhile, the outermost graphene layers could inhibit the direct contact between electrolyte and SnO_x. The performance of SnO_x@G/G in high current density is notable as exhibited in Fig. 4d. The SnO_x@G/G composite is first discharge/charge at 50 mA g^{-1} for 10 cycles, then the rate was increased stepwise to as high as 1000 mA g^{-1}, for 20 cycles at each rate. After 10 cycles at 50 mA g^{-1}, the material maintained a capacity of 920 mAh g^{-1}. At 100 mA g^{-1}, a capacity of 811 mAh g^{-1} is retained, 684 mAh g^{-1} at 200 mA g^{-1}, 533 mAh g^{-1} at 400 mA g^{-1} and 362 mAh g^{-1} at 1000 mA g^{-1}. Furthermore, a capacity of 622 mAh g^{-1} can be recovered once the rate is restored to the initial 50 mA g^{-1}, demonstrating a very good reversibility for the SnO_x@G/G composite. Based on the above data, it can be deduced that the enwrapping of graphene plays a critical part in the SnO_x@G/G composite. Besides, the existing of SnO with a higher theoretical capacity than that of SnO_2 is also important for the good electrochemical performance of SnO_x@G/G.

In summary, a facile layer-by-layer self-assembly approach has been developed to synthesis a sandwich-like graphene wrapped SnO_x@G composite. First, GO in SnO_2@GO acts as a two-dimensional host to permit the homogeneous distribution of SnO_2 nanocrystals. Then, the modification of PDDA can create the positive charged SnO_x@GO, which is very critical for the subsequent GO coating. Besides, it is demonstrated that PDDA is responsible for the transformation from SnO_2 to SnO, although the exact mechanism is still unknown. The final SnO_x@G/G is obtained via the electrostatic interaction between positively charged SnO_x@GO and negatively charged GO, and the simultaneous hydrazine reduction process. The SEM and TEM observations prove that the graphene is effectively coating on SnO_x@graphene. The SnO_x@G/G composite manifests good cyclability and rate capability in lithium ion batteries attributed to the unique sandwich structure, which can avoid the aggregation of the composite and alleviate the volume change of SnO_x during cycling. Besides, the electronic conductivity of the composite can be further improved due to the sandwiched graphene framework. We believe that the proposed synthetic route can be further extended to synthesis of various graphene-wrapped architectures with promising applications in lithium ion batteries, sodium ion batteries, fuel cells, supercapacitors and so on.

Acknowledgement

We acknowledge financial support by the National Nature Science Foundation of China (Grants No 51204209, 51274240).

Notes and references

[a]*School of Metallurgy and Environment, Central South University, Changsha, Hunan, P. R. China. Fax: +86-731-88836329; Tel: +86-731-88710171; E-mail: hncsxyzhou@163.com*
[b]*Department of Mechanical and Engineering, The Hong Kong Polytechnic University, Hong Kong, China. Fax: +86 852-2365 4703; Tel: +86 852-2766 6663.*

† Electronic Supplementary Information (ESI) available: The details of experiment, XRD patterns and TEM image are desribed. See DOI: 10.1039/b000000x/

1 A. Manthiram, *J. Phys. Chem. Lett.*, 2011, **2**, 176-184.
2 E. Peled, C. Menachem, D. Bar-Tow and A. Melman, *J. Electrochem. Soc.*, 1996, **1**, L4.
3 X. Li and C. Wang, *J. Mater. Chem. A*, 2013, **1**, 165-182.
4 V. Etacheri, R. Marom, R. Elazari, G. Salitra and D. Aurbach, *Energy Environ. Sci.*, 2011, **4**, 3243-3262.
5 D. J. Xue, S. Xin, Y. Yan, K. C. Jiang, Y. X. Yin, Y. G. Guo and L. J. Wan, *J. Am. Chem. Soc.*, 2012, **134**, 2512-2515.
6 G. Wang, X. Shen, J. Yao and J. Park, *Carbon*, 2009, **47**, 2049-2053.
7 X. L. Wu, Y. G. Guo, L. J. Wan, *Chem-Asian J.*, 2013, **8**, 1948-1958.
8 T. F. Yi, Y. Xie, Y. R. Zhu, R. S. Zhu, and H. Shen, *J. Power Sources*, 2013, **222**, 448-454.
9 L. Li, A. R. O. Raji and J. M. Tour, *Adv. Mater.*, 2013, **25**, 6298-6302.
10 X. T. Chen, K. X. Wang, Y. B. Zhai, H. J. Zhang, X. Y. Wu, X. Wei and J. S. Chen, *Dalton Trans.*, 2014, **43**, 3137-3143.
11 C. He, R. Wang, H. Fu and P. K. Shen, *J. Mater. Chem. A*, 2013, **1**, 14586-14591.
12 X. Wang, W. Tian, D. Liu, C. Zhi, Y. Bando and D. Golberg, *Nano Energy*, 2013, **2**, 257.
13 X. Li, A. Dhanabalan, L. Gu and C. Wang, Adv. *Energy Mater.*, 2012, **2**, 238-244.
14 X. Wang, Q. Weng, X. Liu, X. Wang, D. Tang, W. Tian, C. Zhang, W. Yi, D. Liu, Y. Bando and D. Golbreg, *Nano Lett.*, 2014, DOI: 10.1021/nl4038592.
15 X. Wang, X. Cao, L. Bourgeois, H. Guan, S. Chen, Y. Zhong, D. Tang, H. Li, T. Zhai, L. Li, Y. Bando and D. Golberg, *Adv. Funct. Mater.*, 2012, **22**, 2682-2690.
16 X. Li, X. Meng, J. Liu, D. Geng, Y. Zhang, M. N. Banis, Y. Li, J. Yang, R. Li, X. Sun, M. Cai and M. W. Verbrugge, *Adv. Funct. Mater.*, 2012, **22**, 1647-1654.
17 C. Zhang, X. Peng, Z. Guo, C. Cai, Z. Chen, D. Wexler, S. Li and H. Liu, *Carbon*, 2012, **50**, 1897-1903.
18 C. A. Bonino, L. Ji, Z. Lin, O. Toprakci, X. Zhang and S. A. Khan, *ACS Appl. Mater. Interfaces*, 2011, **3**, 2534-2542.
19 J. Fan, T. Wang, C. Yu, B. Tu, Z. Jiang and D. Zhao, *Adv. Mater.*, 2004, **16**, 1432-1436.
20 Y. S. Lin, J. G. Duh and M. H. Hung, *J. Phys. Chem. C*, 2010, **114**, 13136-13141.
21 A. K. Geim and K. S. Novoselov, *Nat. Mater.*, 2007, **6**, 183-191.
22 C. Nethravathi, C. R. Rajamathi, M. Rajamathi, U. K. Gautam, X. Wang, D. Golberg and Y. Bando, *ACS Appl. Mater. Interfaces*, 2013, **5**, 2708-2714.
23 J. Liang, W. Wei, D. Zhong, Q. Yang, L. Li and L. Guo, *ACS Appl. Mater. Interfaces*, 2012, **4**, 454-459.
24 Q. Guo, Z. Zheng, H. Gao, J. Ma and X. Qin, *J. Power Sources*, 2013, **240**, 149-154.
25 Y. Yang, X. Ji, F. Lu, Q. Chen and C. E. Banks, *Phys. Chem. Chem Phys.*, 2013, **15**, 15098-15105.
26 J. W. S. Hummers and R. E. Offeman, *J. Am. Chem. Soc.*, 1958, **80**, 1339.
27 S. Wang, D. Yu, L. Dai, D. W. Chang and J. B. Baek, *ACS Nano*, 2011, **5**, 6202-6209.
28 B. P. Vinayan, R. Nagar, V. Raman, N. Rajalakshmi, K. S. Dhathathreyan and S. Ramaprabhu, *J. Mater. Chem.*, 2012, **22**, 9949-9956.
29 A. Dieguez, A. Romano-Rodrguez, A. Vila and J. R. Morante, *J. Appl. Phys.*, 2001, **90**, 1550-1557.
30 S. K. Park, S. H. Yu, N. Pinna, S. Woo, B. Jang, Y. H. Chung, Y. H. Cho, Y. E. Sung and Y. Piao, *J. Mater. Chem.*, 2012, **22**, 2520-2525.
31 J. Y. Park and S. Kim, *Int. J. Hydrogen Energ.*, 2013, **38**, 6275-6282.
32 Y. Wang, Y. Shao, D. W. Matson, J. Li and Y. Lin, *ACS Nano*, 2010, **4**, 1790-1798.
33 M. A. Stranick and A. Moskwa, *Surf. Sci. Spectra*, 1993, **2**, 45-49.
34 Y. Tang, D. Wu, S. Chen, F. Zhang, J. Jia and X. Feng, *Energy Environ. Sci.*, 2013, **6**, 2447-2451.
35 S. Jiang, W. Yue, Z. Gao, Y. Ren, H. Ma, X. Zhao, Y. Liu and X. Yang, *J. Mater. Sci.*, 2013, **48**, 3870-3876.